Journal of Computational Physics 231 (2012) 6643–6664

Contents lists available at SciVerse ScienceDirect

Journal of Computational Physics

journal homepage: www.elsevier.com/locate/jcp

A unified gas kinetic scheme with moving mesh and velocity space adaptation

Songze Chen [a], Kun Xu [a,b], Cunbiao Lee [a], Qingdong Cai [a,*]

[a] State Key Laboratory for Turbulence and Complex Systems, Department of Aeronautics and Astronautics, College of Engineering, Peking University, Beijing 100871, China
[b] Hong Kong University of Science and technology, Clear Water Bay, Kowloon, Hong Kong, China

ARTICLE INFO

Article history:
Received 17 November 2011
Received in revised form 13 May 2012
Accepted 14 May 2012
Available online 15 June 2012

Keywords:
Unified gas kinetic scheme
Rarefied gas
Moving mesh
Adaptive velocity space

ABSTRACT

There is great difficulty for direct Boltzmann solvers to simulate high Knudsen number flow due to the severe steep slope and high concentration of the gas distribution function in a local particle velocity space. Local mesh adaptation becomes necessary in order to make the Boltzmann solver to be a practical tool in aerospace applications. The present research improves the unified gas-kinetic scheme (UGKS) in the following two aspects. First, the UGKS is extended in a physical space with moving mesh. This technique is important to study a freely flying object in a rarefied environment. Second, the adaptive quadtree method in the particle velocity space is implemented in the UGKS. Due to the new improvements in the discretization of a gas distribution function in the six dimensional phase space, the adaptive unified gas kinetic scheme (AUGKS) is able to deal with a wide range of flow problems under extreme flying conditions, such as the whole unsteady flying process of an object from a highly rarefied to a continuum flow regime. After validating the scheme, the capability of AUGKS is demonstrated in the following two challenge test cases. The first case is about the free movement of an ellipse flying at initial Mach number 5 in a rarefied flow at different Knudsen numbers. The force on the ellipse and the unsteady trajectory of the ellipse movement are fully captured. The gas distribution function around the ellipse is analyzed. The second case is about the study of unsteady flight of a nozzle under a bursting process of the compressed gas expanding into a rarefied environment. Due to the strong expansion wave and the huge density difference between interior and exterior regions around the nozzle, the particle distribution function changes dramatically in the particle velocity space. The use of an adaptive velocity space in the AUGKS becomes necessary to simulate such a flow and to control the computational cost to a tolerable level. The second test is a challenge problem for any existing rarefied flow solver.

1. Introduction

To design an accurate unified flow solver in all flow regimes is challenge due to the requirement to resolve different scale flow behavior, i.e., equilibrium and highly non-equilibrium ones. Currently, the direct simulation Monte Carlo (DSMC) method and CFD Navier–Stokes (NS) solvers are two main working horses in rarefied and continuum flow regimes respectively. Practically, the DSMC is the unique and the most reliable method for rarefied flow simulation in aerospace applications [1–3]. On the other hand, in the continuum flow regimes, many accurate CFD-NS flow solvers are available. In the transition

* Corresponding author.
E-mail addresses: jacksongze@tom.com (S. Chen), makxu@ust.hk (K. Xu), cblee@mech.pku.edu.cn (C. Lee), caiqd@pku.edu.cn (Q. Cai).

0021-9991/$ - see front matter © 2012 Elsevier Inc. All rights reserved.
http://dx.doi.org/10.1016/j.jcp.2012.05.019

flow regime between continuum and rarefied ones, both DSMC and NS solvers may have problems. The DSMC is an operator splitting particle based method. In order to validate its physical process in its numerical representation, the cell size and time step in DSMC must be less than the particle mean free path and collision time. Meanwhile, due to the limited number of particles, it takes a long time to reduce the statistic fluctuation, especially for low speed unsteady flow simulations. These features restrict the application of DSMC in near continuum flow regime. On the contrary, the Navier–Stokes equations describe the macroscopic flow evolution with the underlying assumption of small departure from equilibrium states. It is inaccurate to describe non-equilibrium rarefied flows, especially for the phenomena related to heat and boundary. Based on macroscopic description, many other sets of equations have been proposed with the target to improve the performance in transition flow regime, for instant, Grad's 13 moments (G13) [4], regularization of Grad's 13 moments (R13) [5], regularization of Grad's 26 moments (R26) [6], Burnett and super Burnett equations [7], or the direct use of the closed solution of the kinetic model [8]. Even with significant progress, these kind of attempts are not fully successful to calculate the non-equilibrium flows. A NS solution gives a steeper shock structure than those observed in the experiments or the DSMC calculation. The G13 reveals a sub-shock structure. Although the R13 gives a smooth shock profile, its success is still limited to low Mach number cases [9]. Due to Bobylev's analysis, the Burnett and super Burnett equations cannot give a stable shock structure when the Mach number is large [10–12]. Augmented Burnett equations [13] perform better, but these equations are stable only in time, not in space [9].

In order to design a unified scheme for all flow regimes, a natural choice is to combine the advantages of both the DSMC and NS methods. The popular unified method is constructed under the hybrid framework [14–16], where the computation domain is divided into sub-domains with its own valid governing equations. Then, in each sub-domain the flow evolution is simulated by its corresponding solver. Although the hybrid method can work well in continuum and free molecule flow, in the transition flow regime it still has problems. One of the critical questions is about the division of domain, and the validation of both methods around the domain interface. For the hybrid DSMC-NS method, the data interchange between different sub-domains involves new problems. For example, the NS solution is theoretically sensitive to a fluctuating boundary, and non-unique particle distribution functions can be defined from macroscopic flow variables. Indeed, the hybrid method can reveal very sensitive solutions when using different division of domain [17].

Besides the DSMC and NS flow solvers, the Bolztmann equation can be also used directly to construct a unified numerical scheme [18–20]. The Bolztmann equation is supposed to be valid for all flow regimes from continuum to the free molecule flow. Therefore, a direct Boltzmann solver is reasonable approach to design a unified method. The direct Boltzmann solver involves complicated collision integral which costs significantly in its numerical discretization. In order to increase the efficiency, one optional choice is also to develop a hybrid method, such as Boltzmann-NS [21,22]. Another option is to solve a model Boltzmann equation, such as the BGK or Shakhov equations [23–25], instead of the original Boltzmann equation. However, similar to the DSMC, most of the Boltzmann-type solvers use operator splitting approach, which splits the particle movements into free transport and local collision. This kind of splitting limits the time step and cell size of the Boltzmann solver, especially for near continuum flow. Theoretically, it is impossible to design an efficient unified scheme using operator splitting techniques for the transport and collision terms.

The unified gas kinetic scheme (UGKS) [26–28] is newly developed numerical method for all Knudsen number flows. The UGKS is also based on the model Boltzmann equation, but both viscosity and heat conduction coefficients can be set to correct values. The novelty of the UGKS is that a coupled treatment of the particle transport and collision has been used in the gas evolution process, and both macroscopic conservative variables and microscopic gas distribution functions are updated in the scheme. As a result, depending on the intensity of particle collision within a time step the UGKS can automatically recover the hydrodynamic and kinetic scale gas distribution function. Hence, the time step of the UGKS is not restricted by particle collision time. For low transition and continuum flow calculation, the UGKS is more efficient than direct Boltzmann solver and DSMC. Extensive numerical tests have validated the UGKS method, especially for the low speed microflows [29].

The Boltzmann-type solvers always employ a uniform mesh in the particle velocity space. This kind of discretization makes the distribution function based method very expensive for high Mach number and high Knudsen number flow. Owing to the wide spreading of particle velocity distribution in high speed flow and narrow-kernel distribution function at high Knudsen number cases, a mesh in velocity space has to cover an extremely large domain with high resolution. When a uniform mesh is used in the velocity space, the storage and computational load will be unendurable. Moreover, uniform mesh is inefficient to reflect the dramatic changes of distribution function in rarefied high speed flow. In recent years, adaptive velocity space technique has been increasingly used in solving the kinetic equations [30,31]. Kolobov et al. [32,33] introduced the quadtree into the velocity space, and showed the advantages of quadtree structure in solving the collision term of the kinetic equation for the homogeneous flow. It is believed that adaptive mesh has to be used for the Boltzmann solver in the hypersonic rarefied flow simulations. But, for a inhomogeneous flow computation the use of quadtree technique in the Boltzmann solver introduces additional difficulty to keep the momentum and energy conservation during the particle-redistribution process. In this paper, for the first time we are going to construct quadtree technique into the Boltzmann solver for inhomogeneous flow simulation. At the same time, in order to simulate the moving boundary problem accurately and efficiently, we are going to introduce moving mesh method in the physical space into the UGKS as well.

This paper is organized as following. Section 2 presents the implementation of moving mesh and adaptive velocity space methods into the UGKS. Section 3 validates the new scheme through many test cases. Section 4 gives the simulation results of two challenge problems. The first one is an ellipse movement with an initial Mach number 5 at different Knudsen

numbers. The second one is the propelling process of a nozzle and its movement through a rarefied environment. The last section is the conclusion.

2. Adaptive unified gas-kinetic scheme with moving mesh

The philosophical principal underlying the UGKS is to use the partial-differential-equation (PDE) to get a local solution around a cell interface [28], the so-called PDE-based modeling. One of the main reason to use this principal is that the modeled physical scale of the kinetic equation and the numerical scale of a mesh size and time step may be different significantly. A direct discretization according to the PDE, such as using the upwinding method to discretize the transport term in the Boltzmann equation, will introduce physical inconsistent. The Boltzmann equation models the spatial variation of a distribution function in a mean free path scale, and the cell size can be many orders larger than the mean free path. A direct numerical approximation, i.e., $u\partial f/\partial x = u(f_j - f_{j-1})/\Delta x$ for particle velocity $u > 0$, has the following problems. The above discretization means that particles transport across the cell interface freely. If the mesh size is much larger than the particle mean free path, the use of upwinding here is inappropriate, because the particles will take a lot of collisions while they transport through such a long distance in the numerical mesh size scale. The PDE-based modeling is a direct modeling of the gas evolution process in a discretized space around the cell interface. All terms in the kinetic equation, such as transport and collision, will participate in the construction of a local solution. The behavior of this local solution will depend on the ratio between numerical time step Δt and the particle collision time τ. In a highly rarefied regime with a high Knudsen number, due to the fact $\Delta t < \tau$, such as the case in the fully resolved shock layer, a fully non-equilibrium distribution will be maintained. In the limit $\Delta t \gg \tau$, a gas distribution function will converge to the Navier–Stokes solution through the Chapman-Enskog expansion in the continuum regime. In the transition regime with the limit $\Delta t \sim \tau$, the PDE-based modeling will go to a distribution function which accounts for the severe fighting between transport and collision and presents a distribution which can be hardly recovered from a purely analysis of equation because the numerical time step will involve in its evolution. In short, the UGKS is a direct gas evolution modeling in the discretized space, which is not a numerical PDE. Once we use a PDE-based modeling methodology, we are not precisely solving any PDE, but simulate a physical process. The Boltzmann-type models, such as the BGK equation and Shakhov equation, can be used in the UGKS.

The kinetic equation employed by the UGKS can be written in the following form,

$$\frac{\partial f}{\partial t} + \vec{u}\cdot\frac{\partial f}{\partial \vec{x}} = \frac{g^+ - f}{\tau}, \tag{1}$$

where f is particle velocity distribution function which depends on velocity $\vec{u}$, location $\vec{x}$ and time t. For the BGK equation, g^+ is the corresponding local equilibrium state which is a Maxwell distribution,

$$g^+ = g_0 = \rho\left(\frac{\lambda}{\pi}\right)^{\frac{K+2}{2}} e^{-\lambda((u-U)^2+(v-V)^2+\xi^2)}, \tag{2}$$

where U and V are macroscopic velocities of gas, K is the degree of internal freedom and $\lambda = \frac{\rho}{2p}$. Here ρ and p are density and pressure, respectively. Only the monatomic gas in two dimensional case is considered to illustrate the scheme. So the degree of internal freedom K is equal to 1. For the Shakhov equation, g^+ takes the form,

$$g^+ = g_0\left[1 + (1-\mathrm{Pr})\vec{c}\cdot\vec{q}\left(\frac{c^2}{RT} - 5\right)/(5pRT)\right], \tag{3}$$

where $\vec{c} = \vec{u} - \vec{U}$ is peculiar velocity, T is temperature, $\vec{q}$ is heat flux and Pr is Prandtl number. If Pr = 1, the Shakhov model degenerates to BGK model.

The relations between macroscopic quantities with the distribution function f, such as, the density ρ, momentum $(\rho U, \rho V)$, energy ρE, stress p_{ij}, and heat flux q_i are

$$\begin{pmatrix} \rho \\ \rho U \\ \rho V \\ \rho E \end{pmatrix} = \int \psi_\alpha f d\Xi, \quad \alpha = 1,2,3,4, \tag{4}$$

$$p_{ij} = \int (u_i - U_i)(u_j - U_j) f d\Xi, \quad i = 1,2;\ j = 1,2, \tag{5}$$

$$q_i = \int \frac{1}{2}(u_i - U_i)((u-U)^2 + (v-V)^2 + w^2) f d\Xi, \quad i = 1,2, \tag{6}$$

where ψ_α is the component of the vector of moments

$$\psi = (\psi_1, \psi_2, \psi_3, \psi_4)^T = \left(1, u, v, \frac{1}{2}(u^2 + v^2 + w^2)\right)^T \tag{7}$$

and $d\Xi = dudvdw$ is the volume element in the velocity space. Since mass, momentum, and energy are conserved during particle collisions, f and g^+ satisfy the conservation constraint,

$$\int (g^+ - f)\psi_\alpha d\Xi = 0, \quad \alpha = 1,2,3,4, \tag{8}$$

at any location and any time.

Taking the collision time as a local constant, there is a local analytic solution of the kinetic equation which is used for the modeling of gas evolution around a cell interface,

$$f(\vec{x},t,\vec{u},\xi) = \frac{1}{\tau}\int_0^t g^+(\vec{x}',t',\vec{u},\xi)e^{-(t-t')/\tau}dt' + e^{-t/\tau}f_0(\vec{x}-\vec{u}t), \tag{9}$$

where $\vec{x}' = \vec{x} - \vec{u}(t-t')$. The merit to use the above formulation is that this solution covers two scale physical solutions: the hydrodynamic scale behavior from the integration of the equilibrium state and the kinetic scale effect from the initial transport. Physically, the part of the integration of the equilibrium state represents the pressure wave effect in the continuum regime and the initial free transport part gives the individual particle movement effect. In the transition regime, i.e., $t \simeq \tau$, both wave and particle effects will contribute to the gas evolution. This is the main reason for the failure of continuum approach for rarefied flows, where only wave effect is taken into account.

2.1. A brief introduction of unified gas kinetic scheme

The Unified Gas Kinetic Scheme based on kinetic theory is a finite volume method with discrete velocity space. Both macroscopic and microscopic variables in this scheme are updated by conservation law. Even for the update of macroscopic quantities, such as density, momentum and energy, the corresponding fluxes are based on the distribution function which can be a highly non-equilibrium state, such as the case of near free molecule flow. In the UGKS, the whole phase space is discretized. The physical space and velocity space are divided into control volume, i.e., $\Omega_{\vec{x}_i}$ and $\Omega_{\vec{u}_k}$, respectively, where i denotes the index of control volume in physical space and k denotes the index in velocity space. The internal freedom representing the perpendicular velocities can be considered by reduced equations [34], which are solved by the same procedure. The main processes can be summarized below (see Fig. 1):

(1) Suppose the particle distribution function f^n and the macroscopic quantities W^n are known at n time step.
(2) Re-construct the distribution function and macroscopic quantities around the cell interface.
(3) Use the kinetic equation's local solution to construct the time dependent distribution function $f(t)$ for the whole time step.
(4) Evaluate fluxes of both micro and macro quantities through a cell interface.
(5) Use the fluxes to update macroscopic quantities W^{n+1}.
(6) Update the particle velocity distribution f^{n+1} with the inclusion of flux and collision term.

Based on kinetic theory, the flux of any quantity $Q(u)$ in any direction $\vec{n}$ is given in the following form,

$$\mathcal{F} = \vec{n}\cdot\int_{\Omega_{\vec{u}}} \vec{u}fQ(\vec{u})d\vec{u}, \tag{10}$$

where $\Omega_{\vec{u}}$ denotes the integral domain in velocity space, $Q(\vec{u})$ is a functional dependent on the particle velocity. For example, mass flux, momentum flux and energy flux are written as following:

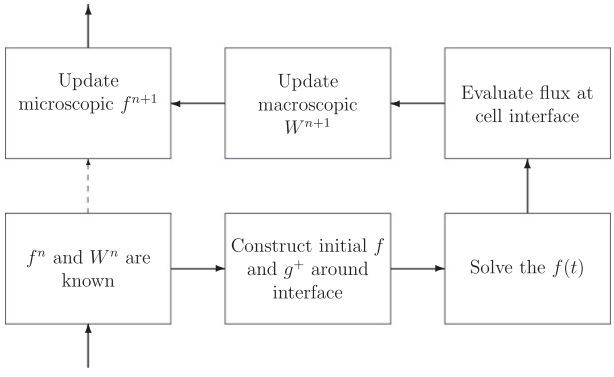

Fig. 1. Basic processes of UGKS.

$$\mathcal{F}_{mass} = \vec{n} \cdot \int_{\Omega_u} \vec{u} f d\vec{u},$$
$$\mathcal{F}_{momentum} = \vec{n} \cdot \int_{\Omega_u} \vec{u}\vec{u} f d\vec{u},$$
$$\mathcal{F}_{energy} = \vec{n} \cdot \int_{\Omega_u} \vec{u} \frac{1}{2} \vec{u}^2 f d\vec{u}.$$

Define the flux of macroscopic quantities,

$$\mathcal{F}_{macro} = \begin{pmatrix} \mathcal{F}_{mass} \\ \mathcal{F}_{momentum} \\ \mathcal{F}_{energy} \end{pmatrix}. \tag{11}$$

The Ω_u denotes the entire velocity space. The flux of a gas distribution function at velocity $\vec{u}_k$ takes the integral only in that sub-volume:

$$\mathcal{F}_{\vec{u}_k} = \vec{n} \cdot \int_{\Omega_{\vec{u}_k}} \vec{u} f d\vec{u}, \tag{12}$$

where the integral is only done for that small control volume around particle velocity $\vec{u}_k$.

The Eq. (9) is employed for the solution of the distribution function at the cell interface, which is used to construct fluxes. The first term of Eq. (9) corresponds to the hydrodynamic scale which should be constructed from macroscopic quantities. The last term can be directly evaluated from the initial distribution function $f_{\vec{u}_k}$. For simplicity, the interface location is denoted as (0,0). The x-direction is the normal direction to a cell interface and the y-direction is along the tangential of the interface. Suppose the initial distribution function takes the following form at a cell interface:

$$f_0(\vec{x}, \vec{u}_k, t)|_{t=0} = f_{0,k}(\vec{x}) = \begin{cases} f^L_{0,k}(0) + \frac{\partial f^L}{\partial \vec{x}} \cdot \vec{x}, & x \leqslant 0, \\ f^R_{0,k}(0) + \frac{\partial f^R}{\partial \vec{x}} \cdot \vec{x}, & x > 0, \end{cases} \tag{13}$$

where nonlinear limiter is used to construct f^L, f^R and their corresponding partial derivatives.

For the integral term of the equilibrium state in Eq. (9), we can use a continuous distribution function to evaluate the integral. For an equilibrium state g^+ around a cell interface, it can be expanded with two slopes [35],

$$g^+(\vec{x}, \vec{u}, t) = g^+(0, u, 0) + g_0[(1 - H[x])a^L x + H[x]a^R x + by + At], \tag{14}$$

where $g^+(0, u, 0)$ denotes the post collision state defined in Eq. (1) and $H[x]$ is the Heaviside function defined by

$$H[x] = \begin{cases} 0, & x < 0, \\ 1, & x \geqslant 0. \end{cases} \tag{15}$$

Here g_0 is a local Maxwell distribution function located at $x = 0$. In the post collision state g^+, a^L, a^R, b and A are related to the derivatives of a Maxwell distribution in space and time. The dependence of a^L, a^R, b and A on the particle velocity can be obtained from a Taylor expansion of a Maxwell distribution function and have the following form,

$$c = c_1 + c_2 u + c_3 v + \frac{1}{2} c_4 (u^2 + v^2 + w^2), \tag{16}$$

where all the coefficients $a^L_1, a^L_2, \ldots, A_4$ are local constants.

As shown in Eq. (2), the g_0 depends on the local macroscopic values of ρ_0, U_0, V_0 and λ_0, which are determined uniquely using the compatibility condition of the BGK model. The conservation constraint at $(x = 0, t = 0+)$ gives

$$W_0 = \int g_0 \psi d\Xi = \sum f_{0,k} \psi = \sum (f^L_{0,k} H[\vec{n} \cdot \vec{u}_k] + f^R_{0,k}(1 - H[\vec{n} \cdot \vec{u}_k]))\psi, \tag{17}$$

where $W_0 = (\rho_0, \rho_0 U_0, \rho_0 V_0, \rho_0 E_0)^T$ is the conservative macroscopic flow variables located at the cell interface at time $t = 0$. Then, the coefficients a^L, a^R and b can be derived through the relation of

$$\left.\frac{\partial W}{\partial x}\right|_{x=0+,y=0,t=0} = \int a^R g_0 \psi d\Xi = M^0_{\alpha\beta} \begin{pmatrix} a^R_1 \\ a^R_2 \\ a^R_3 \\ a^R_4 \end{pmatrix} = M^0_{\alpha\beta} a^R_\beta, \tag{18}$$

$$\left.\frac{\partial W}{\partial x}\right|_{x=0-,y=0,t=0} = \int a^L g_0 \psi d\Xi = M^0_{\alpha\beta} \begin{pmatrix} a^L_1 \\ a^L_2 \\ a^L_3 \\ a^L_4 \end{pmatrix} = M^0_{\alpha\beta} a^L_\beta, \tag{19}$$

$$\left.\frac{\partial W}{\partial y}\right|_{x=0,y=0,t=0} = \int b g_0 \psi d\Xi = M^0_{\alpha\beta} \begin{pmatrix} b_1 \\ b_2 \\ b_3 \\ b_4 \end{pmatrix} = M^0_{\alpha\beta} b_\beta, \tag{20}$$

where the matrix $M^0_{\alpha\beta} = \int g_0 \psi_\alpha \psi_\beta d\Xi$. Using W_0 and the macroscopic quantities at adjacent cells, the derivatives of macroscopic quantities can be obtained by conventional scheme. In order to evaluate coefficient A, we apply the Euler equation $\int_{\Omega_u}((g_0)_t + \vec{u}\cdot(g_0)_{\vec{x}})d\vec{u} = 0$, which govern the equilibrium state, and get

$$M^0_{\alpha\beta}A_\beta = -\int [u(a^L H[u] + a^R(1-H[u]))g_0]\psi d\Xi. \tag{21}$$

With all these coefficients, the hydrodynamic part of the flux is determined in an analytical form. The value of this flux at any point in velocity space can be calculated using the formulation (14) and the flux definition in Eq. (10). Up to this point, the kinetic and hydrodynamic parts of the flux have been constructed.

Based on the physical conservation law, the evolution of macroscopic conservative variables can be obtained. Owing to the conservation in particle collision process, in a discretized space the evolution of macroscopic conservative quantities precisely satisfies,

$$W^{n+1} = W^n + \frac{1}{V_{\vec{x}_i}}\int_{t^n}^{t^{n+1}} \sum_m \Delta S_m \mathcal{F}_{macro} dt, \tag{22}$$

where $V_{\vec{x}_i}$ is the volume of $\Omega_{\vec{x}_i}$ in physical space, ΔS_m is the area of interface and m is index of surfaces of $\Omega_{\vec{x}_i}$.

The update of the distribution function is a little bit complicated. Owing to the collision term and with the update of conservative variables, the conservation law for the distribution function becomes

$$f^{n+1}_{\vec{u}_k} = f^n_{\vec{u}_k} + \frac{1}{V_{\vec{x}_i}}\int_{t^n}^{t^{n+1}} \sum_m \Delta S_m \mathcal{F}_{\vec{u}_k} + \frac{\Delta t}{2}\left(\frac{g^{+(n+1)}_{\vec{u}_k} - f^{n+1}_{\vec{u}_k}}{\tau^{n+1}} + \frac{g^{+(n)}_{\vec{u}_k} - f^n_{\vec{u}_k}}{\tau^n}\right), \tag{23}$$

where trapezoidal rule has been used for the time integration of collision term. Solving the above equation, the f^{n+1} is determined explicitly in the next time level. More detailed formulation can be found in [26,28].

2.2. Moving mesh method in UGKS

The main issue related to the moving mesh method in a physical space is to construct a flux on a moving mesh interface. In the gas kinetic scheme for the continuum flow simulation [36], the traditional procedure is to evaluate the flux in a reference frame fixed on the moving interface, then transform the flux back into a rest reference frame. This kind of scheme includes transformation between two coordinates, which changes the reference frame twice. Following this method, every individual point in velocity space must be transformed four times and the scheme will become complicated.

Indeed, the flux in a rest reference frame can be evaluated directly. Suppose reference frame is a rest frame, and an interface is moving with velocity $\vec{U}_g$. The flux across the interface can be written as below:

$$\mathcal{F} = \int_{\Omega_{\vec{u}_k}} (\vec{u} - \vec{U}_g) f Q(\vec{u}) d\vec{u}. \tag{24}$$

Comparing with the Eq. (10), it is the relative velocity between the particle and interface that determine particle transport across a cell interface. If $\vec{U}_g = 0$, these two formulas are identical. The fluxes for macroscopic quantities and distribution function are given as following,

$$\begin{aligned}
\mathcal{F}_{mass} &= \vec{n}\cdot\int_\Omega (\vec{u} - \vec{U}_g) f d\vec{u},\\
\mathcal{F}_{momentum} &= \vec{n}\cdot\int_\Omega (\vec{u} - \vec{U}_g)\vec{u} f d\vec{u},\\
\mathcal{F}_{energy} &= \vec{n}\cdot\int_\Omega (\vec{u} - \vec{U}_g)\frac{1}{2}\vec{u}^2 f d\vec{u},\\
\mathcal{F}_{\vec{u}_k} &= \vec{n}\cdot\int_{\Omega_{\vec{u}_k}} (\vec{u} - \vec{U}_g) f d\vec{u}.
\end{aligned} \tag{25}$$

The local analytical solution of Eq. (1) on a moving interface is

$$f(\vec{x}, t, \vec{u}, \xi) = \frac{1}{\tau}\int_0^t g^+(\vec{x}', t', \vec{u}, \xi) e^{-(t-t')/\tau} dt' + e^{-t/\tau} f_0(\vec{x} - (\vec{u} - U_g)t), \tag{26}$$

where $\vec{x}' = \vec{x} - (\vec{u} - \vec{U}_g)(t - t')$. It's very similar to the solution (9). The initial distribution function f_0 is the same as the Eq. (13) at cell interface. With this f_0, the kinetic part of flux can be evaluated.

For hydrodynamic part of the flux, the W_0 is required. Consider $f_0(\vec{x} - (\vec{u} - U_g)t)$ at $x = 0,\ t = 0+$, the macroscopic quantities can be determined by conservation constraint,

$$W_0 = \int g_0 \psi d\Xi = \sum f_{0,k}\psi = \sum (f^L_{0,k} H[\vec{n}\cdot(\vec{u}_k - \vec{U}_g)] + f^R_{0,k}(1 - H[\vec{n}\cdot(\vec{u}_k - \vec{U}_g)]))\psi. \tag{27}$$

Then all the coefficients in Eq. (14) can be determined. But these coefficients, as described in previous subsection, are defined in a local coordinate. If we want to implement the flux in global coordinate, a transformation is needed.

In the following part, two coordinates are adopted. the local coordiante follow the interface, moving with $\vec{U}_g$. At an instant, the local coordinate is denoted by (x', y') and is considered as a static coordinate. The x' is a direction normal to the interface. The other coordinate is the global coordinate (x, y). Define the transformation matrix P from global coordinate to local coordinate, which satisfies,

$$(\vec{e}_x, \vec{e}_y)P = (\vec{e}_{x'}, \vec{e}_{y'}), \tag{28}$$

where $\vec{e}$ denotes the unit base vector in the corresponding coordinate. Owing to the orthogonal coordinates used in this scheme, the form of P depends on a single parameter, the intersection angle α between the two coordinates, namely,

$$P = \begin{pmatrix} \cos\alpha, & -\sin\alpha \\ \sin\alpha, & \cos\alpha \end{pmatrix}. \tag{29}$$

Then, the transformation of location and velocity is,

$$(x, y) = (x', y')P^{-1} \tag{30}$$

$$(u, v) = (u', v')P^{-1} \tag{31}$$

Note that the (x', y') and (u', v') are still in the global reference of frame, but with local coordinate system with different orientation relative to global coordinate system for the definition of (x, y) and (u, v).

Given the equilibrium state,

$$g(x', y', t) = g_0(1 + a'x' + b'y' + A't) \text{ in local coordinate } (x', y') \tag{32}$$

and

$$g(x, y, t) = g_0(1 + ax + by + At) \text{ in global coordinate } (x, y). \tag{33}$$

This formula can be expressed in matrix form,

$$\begin{aligned} g(x, y, t) = g0\Bigg[1 &+ (x, y)\begin{pmatrix} a_1 \\ b_1 \end{pmatrix} + (x, y)\begin{pmatrix} a_2, & a_3 \\ b_2, & b_3 \end{pmatrix}\begin{pmatrix} u \\ v \end{pmatrix} + \frac{1}{2}(u^2 + v^2 + w^2)(x, y)\begin{pmatrix} a_4 \\ b_4 \end{pmatrix} \\ &+ t(A_1 + (A_2, A_3)\begin{pmatrix} u \\ v \end{pmatrix} + \frac{1}{2}(u^2 + v^2 + w^2)A_4)\Bigg]. \end{aligned} \tag{34}$$

Substitute the transformations (30), (31) into the above formula, then, derive the transformations for these coefficients

$$\begin{pmatrix} a_1 \\ b_1 \end{pmatrix} = P\begin{pmatrix} a'_1 \\ b'_1 \end{pmatrix}, \tag{35}$$

$$\begin{pmatrix} a_4 \\ b_4 \end{pmatrix} = P\begin{pmatrix} a'_4 \\ b'_4 \end{pmatrix}, \tag{36}$$

$$\begin{pmatrix} a_2, & a_3 \\ b_2, & b_3 \end{pmatrix} = P\begin{pmatrix} a'_2, & a'_3 \\ b'_2 & b'_3 \end{pmatrix}P^{-1}, \tag{37}$$

$$A_1 = A'_1, \tag{38}$$

$$A_4 = A'_4, \tag{39}$$

$$(A_2, \quad A_3) = (A'_2, \quad A'_3)P^{-1}. \tag{40}$$

With the above transformation, the hydrodynamic part of the flux $f_{\vec{u}_k}$ can be evaluated in a global coordinate directly.

To implement the conservation law, the same method as used in standard UGKS is adopted to evaluate the collision term and update the new quantities for next time step (see Eqs. (22) and (23)).

2.3. Adaptive velocity space in UGKS

The moving mesh method presented in last subsection improves the applicability of the UGKS. However, in order to increase the efficiency of the UGKS, an adaptive velocity space must be adopted. For Vlasov equation, Lagrangian adaptive and quadtree adaptive methods have been implemented in phase space in [30,31]. In the adaptive process, for the Boltzmann equation without external force, the conservation law must be carefully maintained, especially in the process of redistributing the particles in the velocity space. For the UGKS, the update of conservative macroscopic quantities also effect the distribution function through the collision term. Indeed, Ref. [32] only concentrates on evaluation of the collision term in quad/octree adaptive velocity space, without touching the transport part.

Considering the complexity of distribution function for high Knudsen number, quadtree mesh in velocity space is implemented in this study. Since the collision term of the modeling equation is much simpler than the Boltzmann equation, we will focus on solving convection part of the equation.

Fig. 2 illustrates the configuration of full quadtree structure and quadtree mesh. The leaf node in quadtree structure corresponds to the cell in quadtree mesh. The depth of a node k is D_k, which denotes the length of the path from the root to this node. And the subtree height is presented by H_k, which denotes the length of the path from the root of subtree to the deepest node in the subtree. In Fig. 2, the vertical line between the two quadtree presents the interface in physical space. Since the quadtrees are different at different location, the forest of several quadtrees should be always considered in new scheme. We define the counterpart subtree whose root shares the same path from the root of each quadtree to the root of subtree in the forest. In this study, the distribution function is defined at leaf node, i.e., the cell center in velocity mesh. Under this definition, the distribution function can be regarded as the average particle number density in the cell, or, the particle density at cell center. Moreover, all particles in the cell k are with the same average velocity $\vec{u}_k$. As shown in Fig. 2, the particles on the left travel to the right. These particles with four different velocities, $\vec{u}_{k1}$, $\vec{u}_{k2}$, $\vec{u}_{k3}$, $\vec{u}_{k4}$, must be presented on their counterpart of right quadtree mesh which has only one velocity here. This means that four kinds of particles will merge into one kind of particles. It is easy to notice that this kind of merging process, or its inverse splitting process, will violate the conservation law. This kind error should be controlled through error estimation.(i) Error estimation.

In this part, the error induced by emerging and diminishing of particles will be estimated through the analysis in one dimension. Suppose particles on the left, which correspond to velocity distribution function $f_0(u_0)$ on level D_0, travel to the right adjacent cell and split into two kinds of particles with velocity distribution functions $f_+(u_+)$ and $f_-(u_-)$ on level D_0+1. The cell size in velocity space of level D_0 is $2\Delta u$. With the definition $\Delta f = f_+ - f_-$, to keep the mass conservation requires $f_+ = f_0 + \frac{1}{2}\Delta f$ and $f_- = f_0 - \frac{1}{2}\Delta f$. The difference between two fluxes affecting both sides can be written in a uniform form,

$$\Delta f \Delta u C + \Delta u P(\Delta u), \tag{41}$$

where P denote polynomials of Δu and C denotes a constant. The leading order is $O(\Delta u)$ related to Δf. Since the flux for macroscopic variable is the summation of the flux in velocity space, the error of macroscopic flux depends on the cell size Δu and the variation f on level D_0+1. As implied by Eq. (41), there are two means to reduce the error, i.e., keeping the velocity mesh on the same level or refining velocity mesh.

(ii) Singularity of gas distribution function in highly rarefied case.

Theoretically, the use of the same grid and refining the mesh size can reduce the error induced in the splitting and merging process. However, the steep slope of the particle distribution function makes the later method impratical. Suppose that a distribution function is continuous, then $\Delta f = \Delta u \frac{\partial f}{\partial u} + O((\Delta u)^2)$. Considering the 1D collisionless Boltzmann equation, the analytical solution is,

$$f(x,u,t) = f_0(x-ut,u), \tag{42}$$

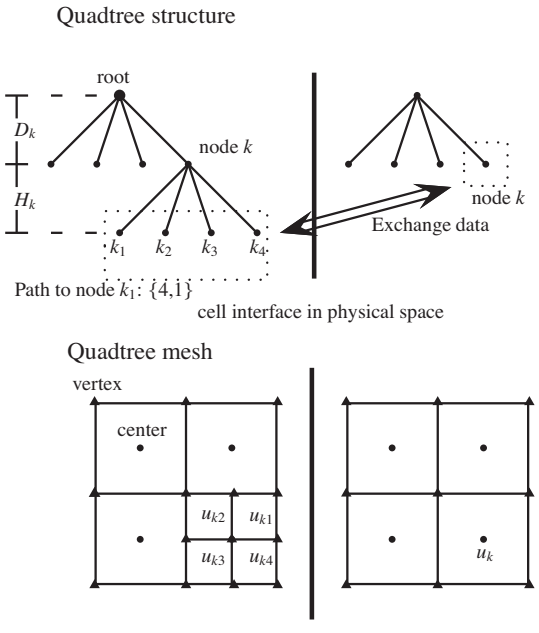

Fig. 2. Illustration of quadtree data structure.

where the f_0 is initial distribution. Take partial derivative of f for variable u,

$$\frac{\partial f}{\partial u} = \frac{\partial f_0}{\partial u} - t\frac{\partial f_0}{\partial x}. \tag{43}$$

The expression of $\frac{\partial f}{\partial u}$ indicates that partial derivative will diverge when time goes to infinity unless f is homogeneous function in physical space. Due to the free transport mechanism of the collisionless Boltzmann equation, this phenomenon for creating large gradient of $\partial f/\partial u$ is understandable. In other words, it is a distinguished feature of free molecule flow that particles travel with their own velocities individually and there is no connection between these particles even the velocities of these particles are very close. The $\Delta u\frac{\partial f}{\partial u} \sim \Delta f$ can not decrease to zero while the Δu go to zero in collisionless flow. The corresponding distribution function might be described by a generalized function. Fortunately, the collision term can eliminate this singularity and keep the distribution function regular in real gas system.

However, as the Knudsen number increases, the molecular collision becomes weak, the singular effect in the distribution function arises gradually. It leads to the failure of the method even with velocity mesh refining, i.e., the Δf might get so large that it requires very small cell size in velocity space to control the error under a certain level. It is impractical to reduce the error through constantly refining of a uniform velocity mesh. And, furthermore, like things happen on staggerd mesh, the error will accumulate while the particles travel on different velocity meshes. Therefore, the counterparts of quadtrees at different locations must keep in the same level unless there are few particles (small velocity distribution function) in this velocity element.

As a consequence, constraints must be adopted while refining velocity mesh. Obviously, to develop a global and general quadtree mesh method is preferred, but may get too cumbersome. Here we propose several constraints for the local mesh refinement in velocity space. The criterion of splitting and merging process will be chosen according to the parameters defined by $M_1 = f_{\vec{u}_k}(\Delta u_k)^2/\rho$ and $M_2 = \frac{1}{2}(\vec{u}_k - \vec{U})^2 f_{\vec{u}_k}(\Delta u_k)^2/\left(E - \frac{1}{2}\rho\vec{U}^2\right)$, namely, the percentage of particles within velocity element $\Omega_{\vec{u}_k}$ and the corresponding contribution to the thermal energy. They are defined at leaf-nodes or parent-nodes of leaves.

(a) The difference between depth of the counterpart subtrees is less than 2 at adjacent locations.
(b) When M_1 and M_2 are larger than a certain value, say, C_2, the adjacent counterpart subtrees keep in the same height.

A possible route for mesh refinement in velocity space is given as following.

(0) The initial quadtrees of velocity space at all locations are identical and satisfy the constraints, (a) and (b), then the particle distrition function changes.
(1) Traverse all the leaf-nodes and the parent-nodes of leaves of the current quadtree.
(2) If M_1 or M_2 of the leaf-node is larger than threshold C_1 and the height of counterpart subtree of every adjacent location is not less than 0, the leaf-node splits. (If no subtree in a quadtree can follow a given path, set a minus heihgt to the depth of subtree.)
(3) If the height of counterpart subtree of any adjacent location is bigger than 0 and M_1 or M_2 of the leaf-node or the root of the counterpart subtree is bigger than the threshold C_2, the leaf-node splits.
(4) If the height of counterpart subtree of any adjacent location is bigger than 1, the leaf-node splits.
(5) If M_1 and M_2 are small enough for parent-node, say, smaller than a threshold C_3 and the height of counterpart subtree of every adjacent location is not more than 1, the parent-node merges.
(6) If any of $(2 \sim 5)$ are satisfied during the traversing, repeat from (1).

By following these rules, the constraints (a) and (b) are satisfied. Actually, the particle distrition function changes much slowly than the velocity mesh during the caculation. According to our numerical experience, traversing the quadtree once in each time step is sufficient for the adaption. As analyzed before, the error due to the splitting and merging process can be restrained on a small level as long as the C_2 takes an appropriate value. Meanwhile the rules (2) and (5) make the mesh tracking the particles in velocity space.

2.4. Boundary condition

(i) Solid boundary.

There are two kinds of solid boundary, i.e., the specular reflection and diffusive reflection. For specular reflection, the velocities of the particles reflected by solid boundary do not always fall on the grid in velocity space except some special cases. Hence, this will involve interpolation of distribution function on the velocity grid. The easiest specular reflection boundary case is that the solid boundary are parallel to the axis of the coordinate and the velocity grid are symmetric about the origin. For diffusive reflection, a general case is considered. Without loss of generality, assume that the gas is on the left of the boundary and the solid wall is on the right. The distribution function of gas is f^L, and the distribution function of the particles emitted from the solid wall can be presented by a Maxwell distribution function,

$$g^W = \rho^W\left(\frac{\lambda^W}{\pi}\right)^{\frac{K+2}{2}} e^{-\lambda^W((u-U^W)^2+(v-V^W)^2+w^2)}. \tag{44}$$

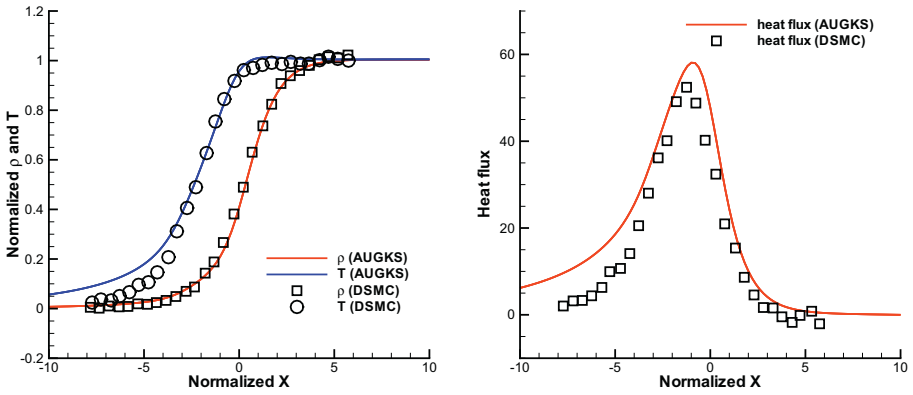

Fig. 3. Shock structure for $M_s = 8$, and $\mu \sim T^{0.68}$.

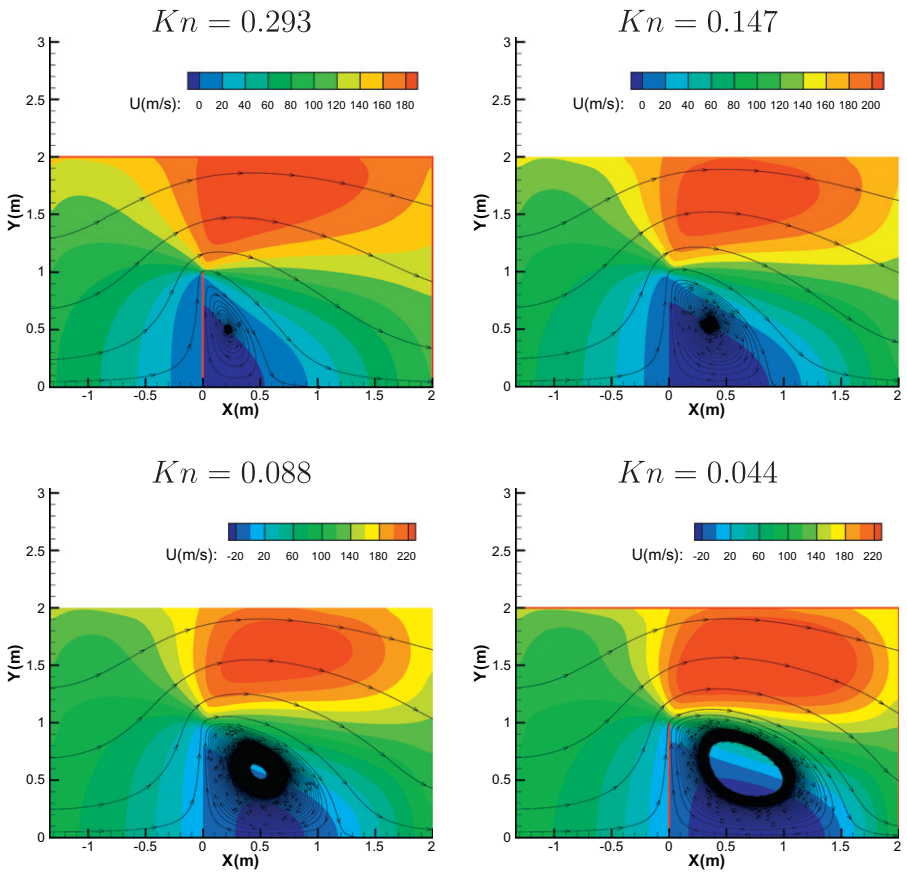

Fig. 4. The contour of U velocity and the streamline.

The λ^W and $\vec{U}^W$ are given as the boundary condition. Then no penetration condition is used to determine ρ^W, i.e.,

$$\vec{n} \cdot \int_{\vec{n}\cdot(\vec{u}-\vec{U}^W)\geqslant 0} (\vec{u}-\vec{U}^W) f^L d\vec{u} = \vec{n} \cdot \int_{\vec{n}\cdot(\vec{u}-\vec{U}^W)<0} (\vec{u}-\vec{U}^W) g^W d\vec{u}. \tag{45}$$

(ii) Inlet and outlet boundary.

As the flow regime varies in a wide range, the inlet and outlet boundary should also cover a wide range of flow regime. The flow can be categorized into two kinds of flows by the Mach number, supersonic flow and subsonic flow. Under these categories, Riemann invariants can be used to construct the quantities on the boundary. However, when the Knudsen

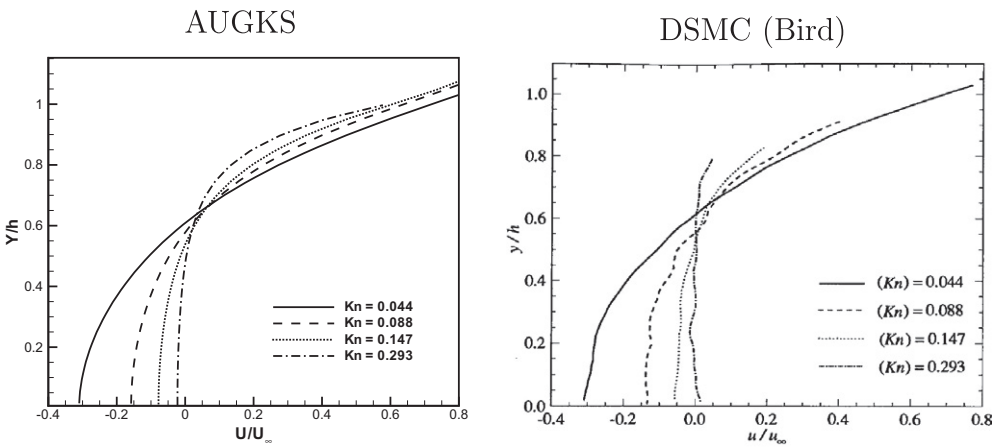

Fig. 5. The profile of U velocity along the verticle line through the center of vortex.

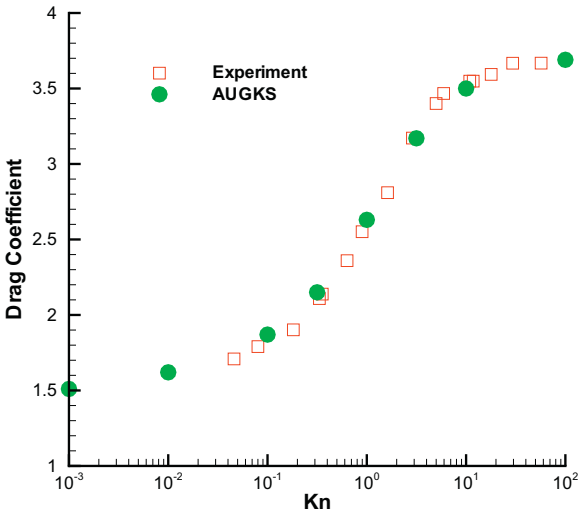

Fig. 6. Drag coefficient vs Knudsen number.

number becomes large, the Euler and Navier–stokes equations are invalid. As a result, the boundary condition based on Riemann invariants is inaccurate for rarefied flow. Therefore, we propose a semiempirical boundary condition to present the rarefied effect. A global Knudsen number is used to construct a weight function $\alpha = e^{-1/\mathrm{Kn}}$. The uniform incoming flow are presented by W_∞, and the macroscopic quantities constructed by Riemann invariants are denoted by W_R. Then the macroscopic quantities on the boundary is constructed as,

$$W_b = \alpha W_\infty + (1-\alpha) W_R. \tag{46}$$

In the two limiting cases of free molecular and continuum flow, the above boundary condition is consistent with traditional approach. Meanwhile, the above formulation provides a smooth transition connecting the limiting cases, and works very well.

3. Numerical validation

1 D and 2 D test cases are used to validate the new scheme. All the results are calculated using the same program.

3.1. Shock structure

The shock structure is typically a non-equilibrium flow structure. Capturing this structure is a basic requirement for any flow solver for rarefied flows. To examine new scheme, a Mach 8 moving argon shock structure is computed by AUGKS, and its result is compared with the DSMC solution [37]. Fig. 3 shows the shock structures for viscosity coefficient $\mu \sim T^{0.68}$, where

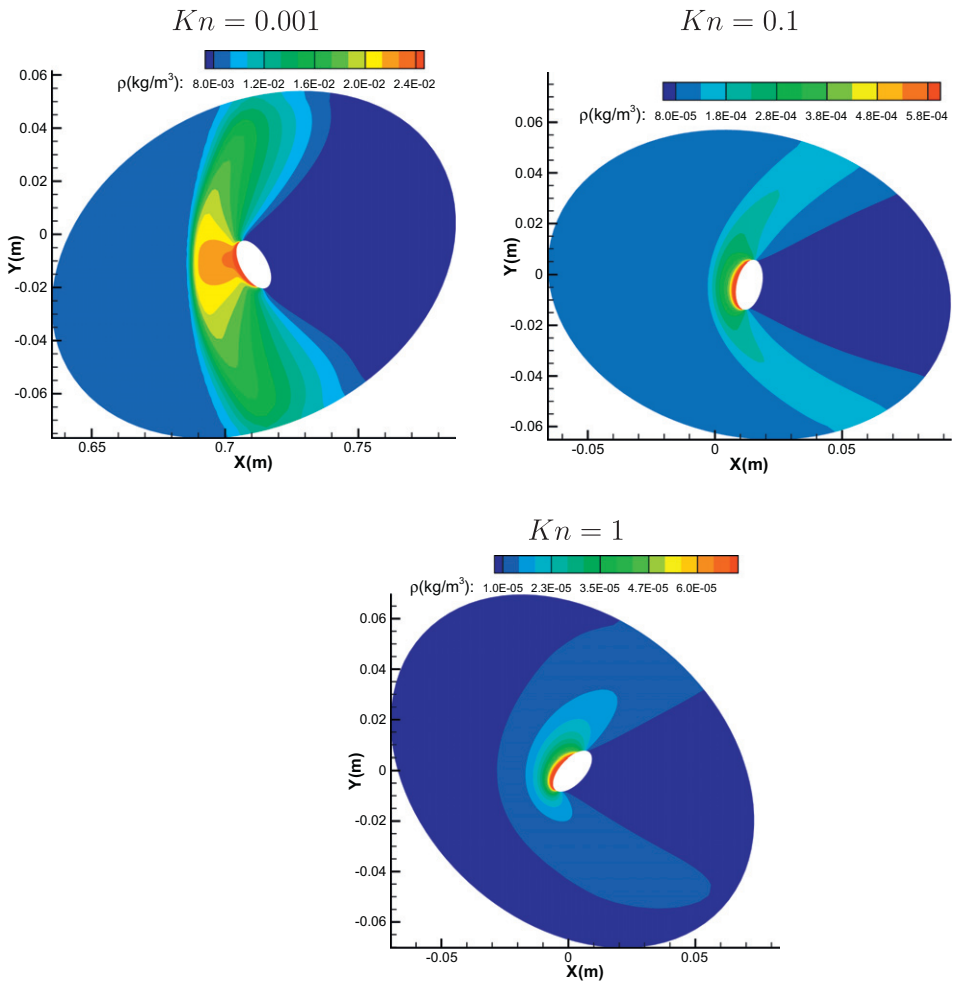

Fig. 7. The density field for shock driven ellipse.

the x-coordinate is normalized by $\sqrt{\pi}l_0/2$ and l_0 is the mean free path of the gas molecules at the upstream condition. For this Mach 8 case, the shock thickness and the separation distance between the density and temperature profiles by AUGKS compare well with those of early DSMC solution.

3.2. Flow past vertical plate

A vertical plate is placed in a uniform flow. The vortices behind the plate vary as a function of Knudsen number. Owing to the simple geometry and boundary conditions, Bird [3] has used this case to illustrate the rarefied effect. The incoming flow has a speed of $U = 172m/s$. The stream temperature is 300 K, and the corresponding Mach number is about 0.53. The vertical plate is located at $x = 0m$ and the boundary condition is assumed to be sepcular reflection. A symmetric boundary which is equivalent to sepcular reflection is imposed at $y = 0m$. The semi-height of plate h is 1, the inlet boundary is at $x = -4/3m$, the outlet boundary is at $x = 2m$, and the upper boundary is at $y = 2m$. As defined by Bird [3], these boundaries use the 'stream' boundary condition, such that the outgoing molecules are discarded, and the incoming molecules are the undisturbed initial stream at these boundaries. The flow structures are shown in Fig. 4. The profile of the U velocity along the center of vortex are shown in Fig. 5 for different Knudsen numbers. As the Knudsen number decreases, the vortex becomes stronger and the length of the wake increases. Our results are very similar to Bird's, and there are no oscillation in velocity plot. However, we must emphasize that the results are derived under specific computational domain and boundary conditions. As discussed by Bird, the wake length would be much longer than current results when the computational domain is enlarged.

3.3. Drag coefficient of cylinder in the whole transition flow regime

The drag coefficients of a cylinder are calculated by AUGKS for a wide range Knudsen numbers. The results are compared with the experimental data [38]. Monatomic gas is chosen as the medium with Prandtl number Pr = 2/3, ratio of specific

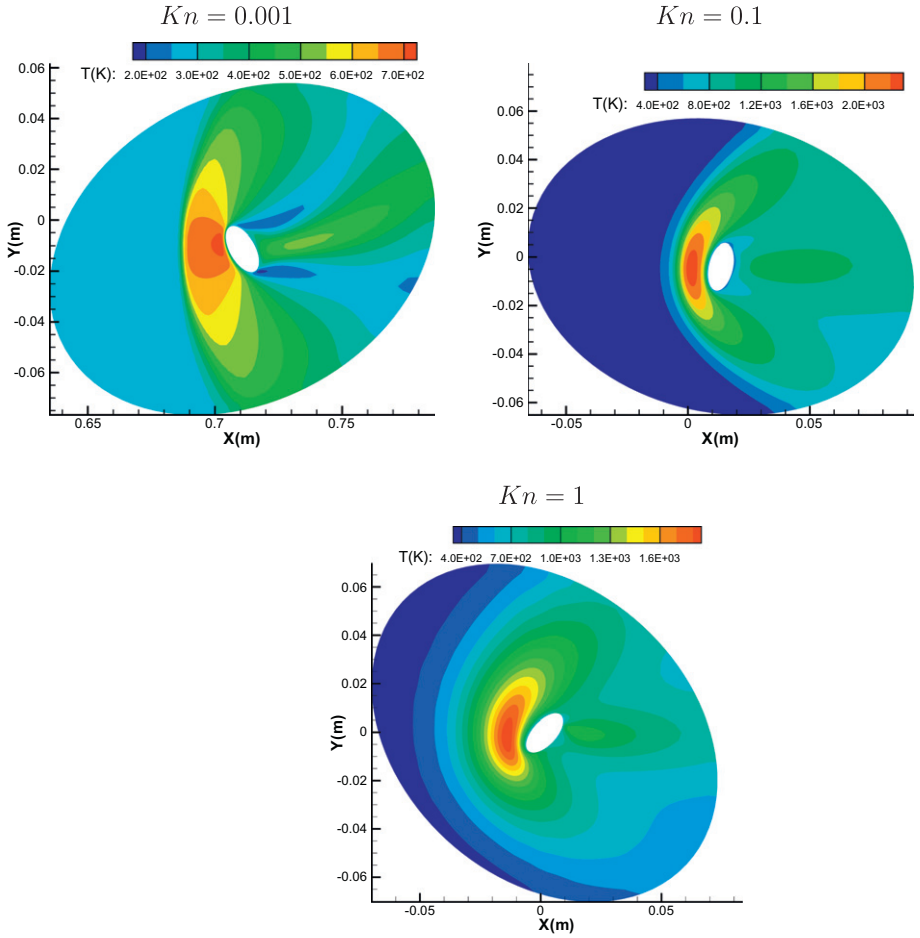

Fig. 8. The temperature field for shock driven ellipse.

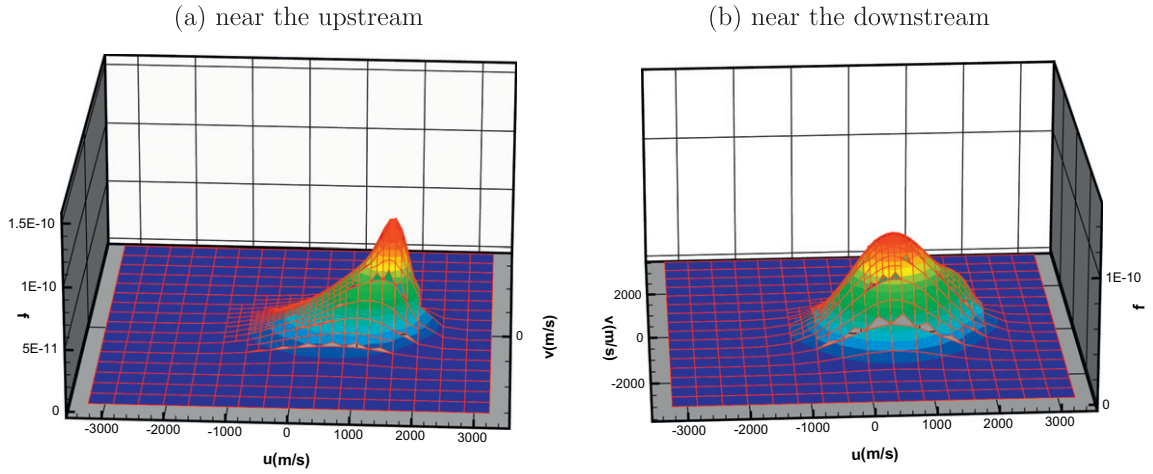

Fig. 9. The velocity distribution function inside the shock for Kn = 0.1.

heats $\gamma = 5/3$. The Mach number of incoming flow is 1.96. And the range of Knudsen numbers is from 0.001 to 100. The diameter of cylinder is denoted by D, and the diameter of whole computational domain is $11D$. The inlet and outlet boundary defined in last subsection is applied in this case. And the wall boundary condition is diffusive reflection. The mesh used in

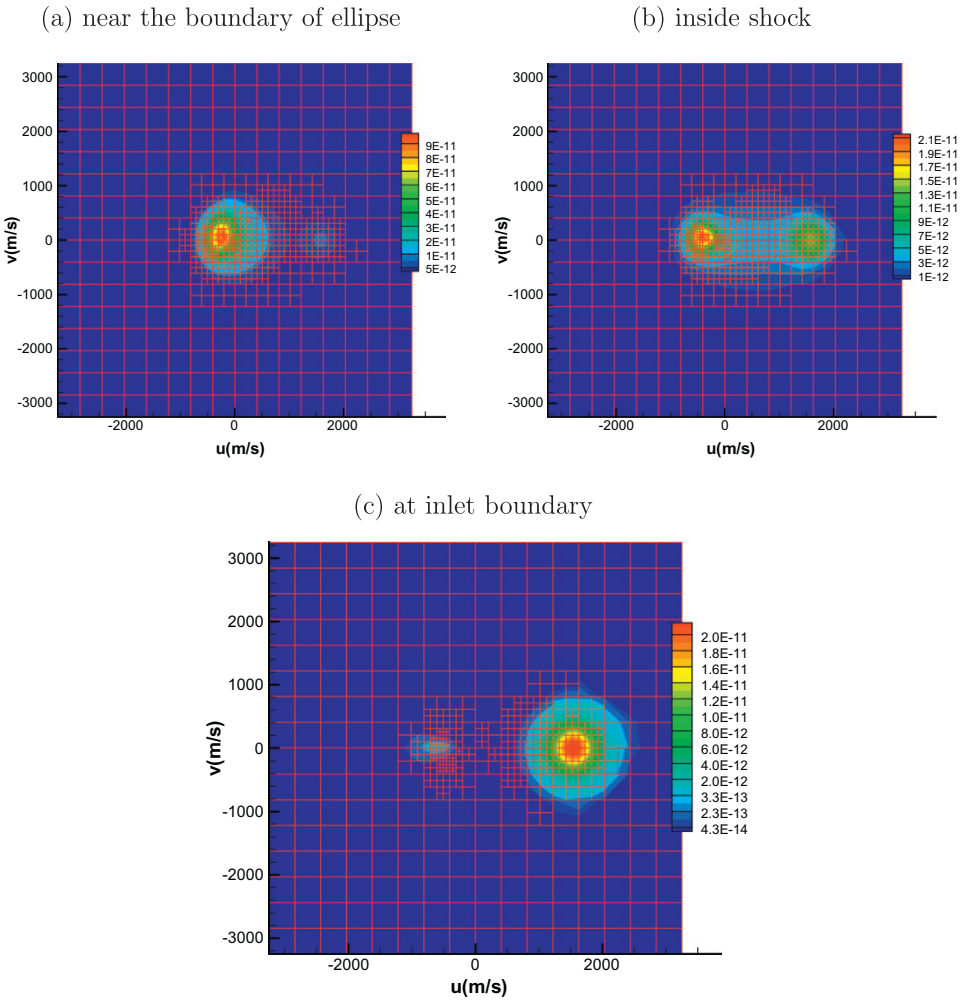

Fig. 10. The velocity distribution function through the shock for $Kn = 1$.

physical space is 100×60. The initial quadtree mesh is 16×16, which are controlled by $C_1 = 0.04$, $C_2 = 1 \times 10^{-4}$ and $C_3 = 1 \times 10^{-7}$. The wall temperature T_w is updated dynamically through the heat transfer from the flow (denoted by Q). Specifically, given the thermal capacity of the cylinder C, the temperature change is

$$\frac{\partial T_w}{\partial t} = \frac{Q}{C}, \tag{47}$$

where Q is obtained by the AUGKS, and C is a given appropriate value by numerical experiments. Actually, the value of C only determines how fast the T_w goes to a steady state, but doesn't affect the final result. The final T_w is determined only by the heat flux Q computed by AUGKS, which will go to zero when the temperature of the cylinder rises. Fig. 6 shows the numerical result and the experimental data.

4. Numerical experiments with AUGKS

In this section, we are going to apply the AUGKS method to two challenge rarefied flow problems. The first one is a freely moving ellipse inside a hypersonic flow of different Knudsen numbers. This case is a common issue encountered in astronautical application. The particle distribution function changes dramatically from the upstream to the downstream. The simulation will be done with the moving physical mesh and adaptive velocity space. For different Knudsen numbers, the force and torque on the ellipse will be calculated to determine the flight trajectory of the ellipse. During the transport process, the distribution function shows singularity behavior. The second case is about the exhausting flow from a nozzle and the nozzle's movement. Owing to the huge density difference between the exterior and interior regions around the nozzle, the flow covers from the continuum to the transition regimes. For this simulation the use of the UGKS with a uniform mesh in velocity space will be extremely expensive, because the very low temperature induced through the rapid expansion will confine the

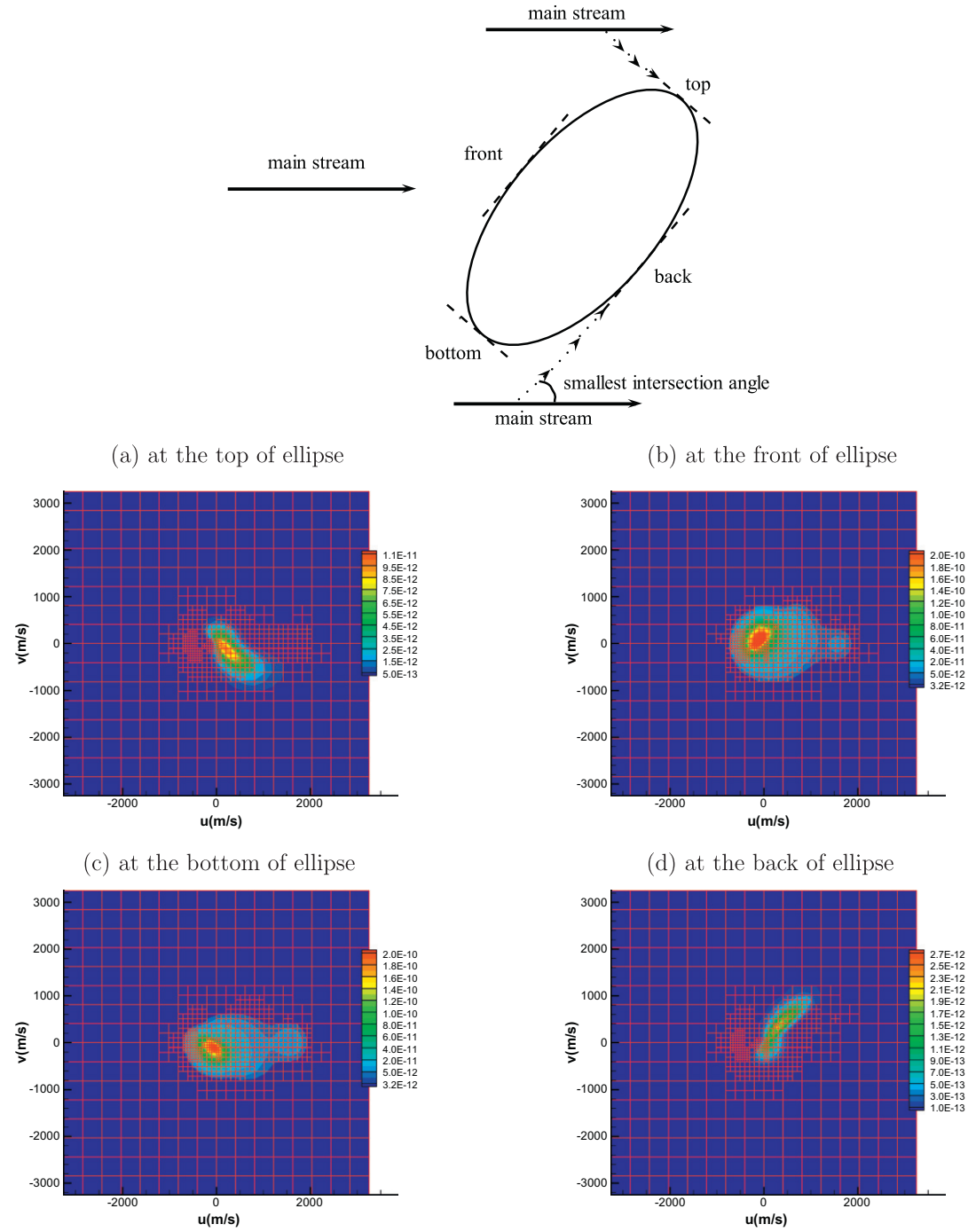

Fig. 11. The velocity distribution function near the wall boundary for $Kn = 1$.

particle distribution function mainly in a narrow area in velocity space. These two problems are considered in 2 dimension. And the length in the third dimension is regarded as $1m$. The new inlet and outlet boundary defined in Section 2.4 is applied in these two cases. And the wall boundary condition is diffusive reflection.

4.1. Moving ellipse inside a hypersonic rarefied flow

A freely moving ellipse rests initially in a flow with velocity of $1538.73m/s$, temperature of $273K$, and dynamic viscosity of $2.117 \times 10^{-5}\ m^2/s$. The center of ellipse locates at $(0, 0)$ and the angle of attack of the ellipse is $-45°$ when the calculation

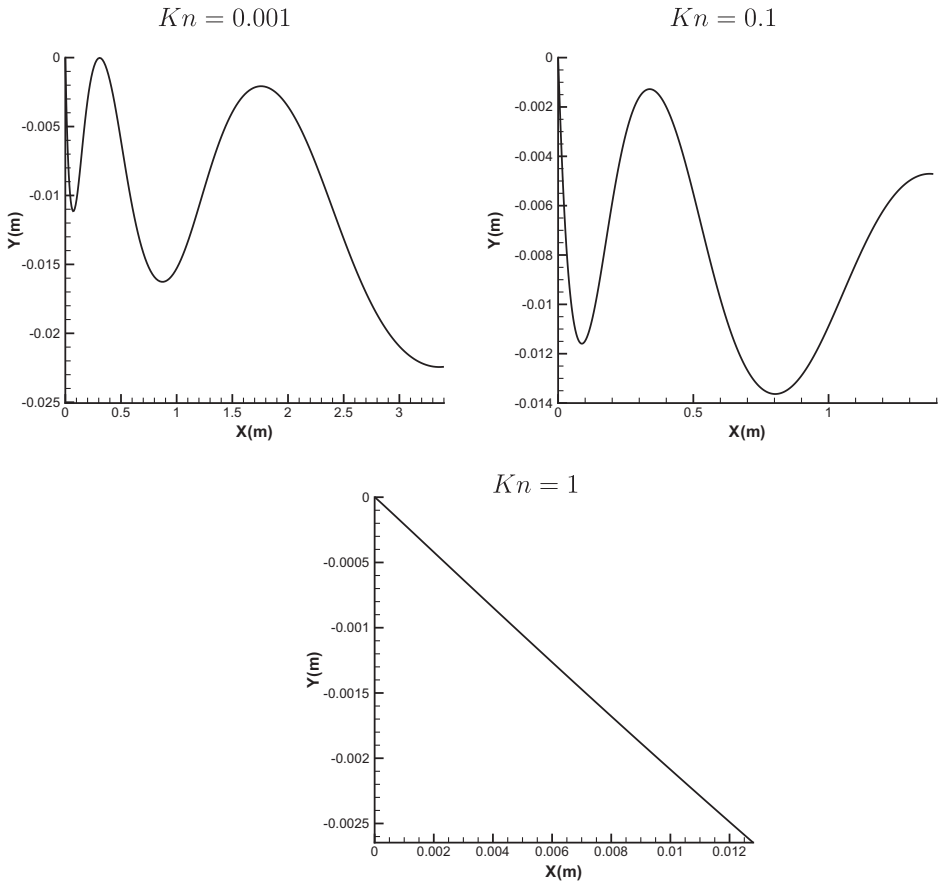

Fig. 12. The traces of ellipse center in $Ma = 5$ hypersonic flow.

starts. The incoming flow has a Mach number 5. Three cases with different upstream densities, i.e., $8.582\times 10^{-3}\ kg/m^3, 8.582\times 10^{-5}\ kg/m^5$, and $8.582\times 10^{-6}\ kg/m^3$, are calculated. The corresponding Knudsen numbers are 0.001, 0.1, 1, respectively. The long axis of the ellipse is 0.02 m and the short axis is 0.01 m. In order to get visible displacement during simulation, the density of ellipse is relatively small, say, 1 kg/m^3. The force and torque on the ellipse are calculated during the flight, which determine the ellipse's flight trajectory and its rotation.

Figs. 7 and 8 show the density and temperature field at $t = 1.28\times 10^{-3}\ s$. At Kn = 0.001 case, similar to shock capturing scheme for continuum flow, the AUGKS presents a sharp shock front. The gas distribution functions are very close to Maxwell distribution in the whole computational domain expect at the shock front and close to the boundary. As the Knudsen number increases, the shock thickness gets broaden and the shock structure becomes resolved. For example, at $Kn = 0.1$, the shock thickness is comparable with the size of the ellipse. The distribution functions inside the shock becomes non-equilibrium states, which are shown in Fig. 9. At $Kn = 1$, the dissipative shock layer extends almost to the whole upstream region. As suggested by the Mott-Smith approximation [39], a bimodal type distribution function shows up in the shock region, see Fig. 10. Even close to the inlet boundary, this bimodal still exists in Fig. 10(c).

Examining the distribution function near the wall, the computation shows that the distribution function on the upwind side has a bimodal type (see Fig. 11(b, c)), and the distribution function on the downwind side is of a banded structure (see Fig. 11(a, d)). The bimodal distribution function on the upwind side suggests two sources of particles, one is from the upstream and the other is reflected from the wall. But, for the banded distribution function the interpretation is not so straightforward. Theoretically, there are three possible particle sources composing of the banded distribution function, namely, the free transport, wall reflection, and scattering due to the molecular collision. Based on the highly non-equilibrium shape of the distribution function, the collision effect will not play important role and can be excluded. If the wall reflection part contributes mostly, there should be a peak around zero velocity, which is similar to the cases shown in Fig. 11(b, c). Moreover, the distribution band is almost along a $\pm 45^\circ$ line which is the tangential direction of the corresponding wall boundary. Considering all these facts, we suggest that the banded distribution function is mainly formed from the free transport along the tangent line of the boundary. Indeed, for high Mach number and high Knudsen number flows, the backward moving particles are extremely rare. So, the most particles which can arrive at the downwind side are moving along the line which has the smallest intersection angle with the main stream direction. Examining the banded distribution function carefully, a small

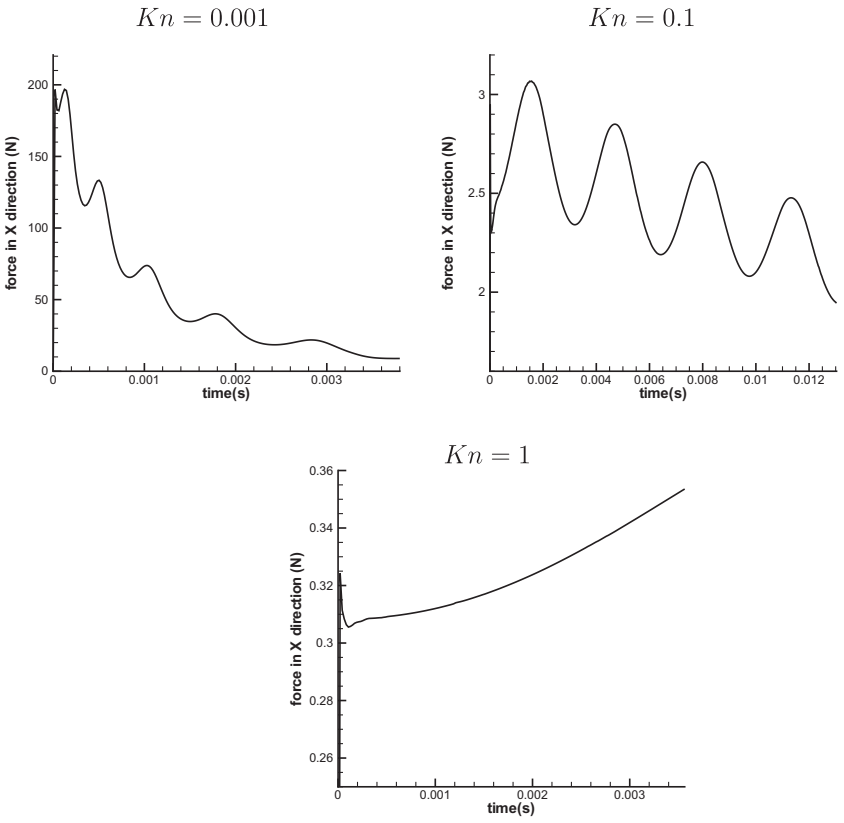

Fig. 13. The force in x direction of shock driven ellipse.

twist can be observed around zero velocity in Fig. 11(a, d). The twisted part of distribution function corresponds to the velocity normal to the main direction of the banded distribution, namely, normal to the boundary. It suggests that these particles are coming from the wall. As a result, this small twist could be interpreted by the wall reflection.

Figs. 12–14 show the traces of the ellipse center, the forces in x direction and torques in different cases. The force applied on the ellipse decreases as the Knudsen number increases. This phenomenon attributes to the decrease of gas density. The Mach number M, flow rarefaction Kn, and the density ratio of the ellipse over the surrounding gas determines the rich dynamics of the ellipse movement.

4.2. Expansion flow from a nozzle

The nozzle is designed to have a rectangle shape with a round head. Fig. 15 gives the nozzle's configuration and the initial position and attitude. The mass of the nozzle is 1.57×10^{-2} kg. Both the dense gas inside the nozzle and the dilute gas outside the nozzle are stationary initially. The temperature is 273 K for all gas and solid walls. Density inside the nozzle is $\rho_{in} = 8.582 \times 10^{-2}$ kg/m^3, and $\rho_{out} = 8.582 \times 10^{-6}$ kg/m^3 outside, with viscosity coefficient 2.117×10^{-5} m^2/s. The Knudsen number of the external gas is 0.05, based on the diameter of head. The whole expansion consists of three stages. Initially, the gas exhausting from the nozzle. In this stage, the gas behaves as a free expansion. Since the external gas is so dilute, the dense gas expansion meets almost no resistance from environment gas. The stream lines become radial, see Fig. 16. Associated with the intensive expansion, the temperature of gas drops quickly to almost 10 K. The distribution function becomes a narrow-kernel shape in the velocity space. After free expansion, a jet appears behind the nozzle. Owing to the reduced density difference outside, the follow-up gas out of the nozzle is confined in a narrow region. Fig. 17 shows the flow field. At the same time, due to the re-action force from the expansion, the nozzle gets accelerated and then moves by its own inertia. Eventually, the expansion stage terminates. Fig. 18 shows that the pressure inside the nozzle is lower than the surroundings. The streamline around the nozzle presents a typical characteristic flow at low speed. Because the environment density is very low, the deceleration is very weak. This stage will sustain a long time until the nozzle gets stopped.

Fig. 19 shows the quadtree mesh and contour of particle distribution function at the middle of the right outlet during the expansion stage. At first the distribution function keeps a Maxwell distribution (Fig. 19(a)). Then the fast particles arrive, and distort the distribution function a little bit (Fig. 19(b)). The corresponding macroscopic picture shows that a shock wave

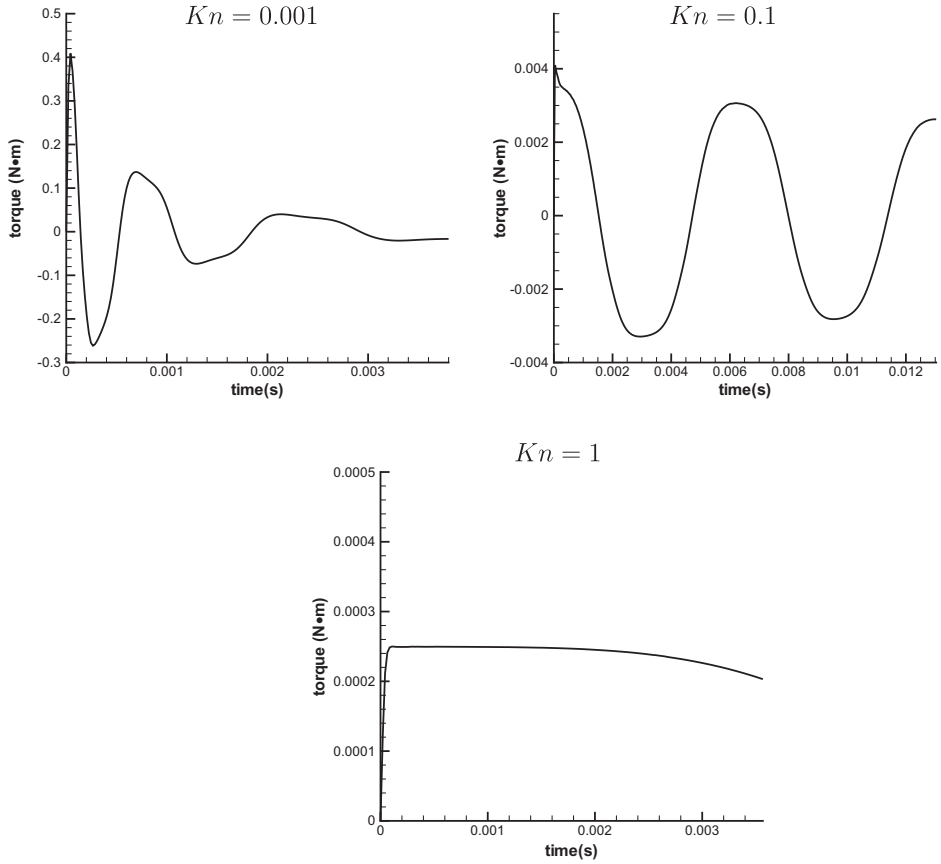

Fig. 14. The torque of shock driven ellipse.

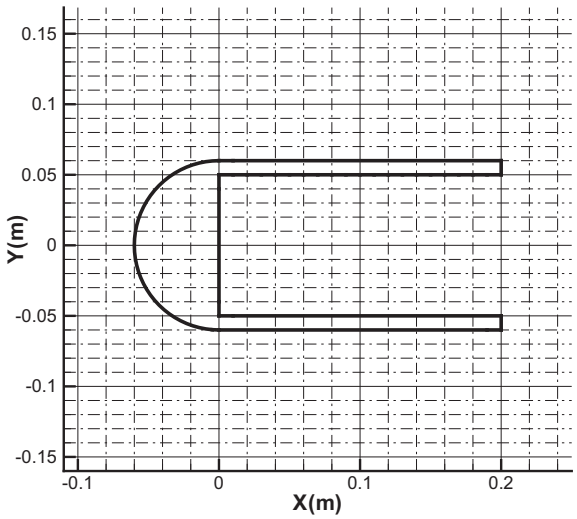

Fig. 15. The configuration of nozzle.

sweeps this location. The followed expansion makes the temperature drop significantly to a very low value. As shown in Fig. 19(c), the kernel of distribution function becomes much more concentrated than the initial one.

Fig. 20 presents a series of moving velocity of the nozzle and absolute *x*-direct force on it. In the plot of absolute force magnitude, the circles present the thrust (negative force) and the squares give the drag (positive force). The max velocity

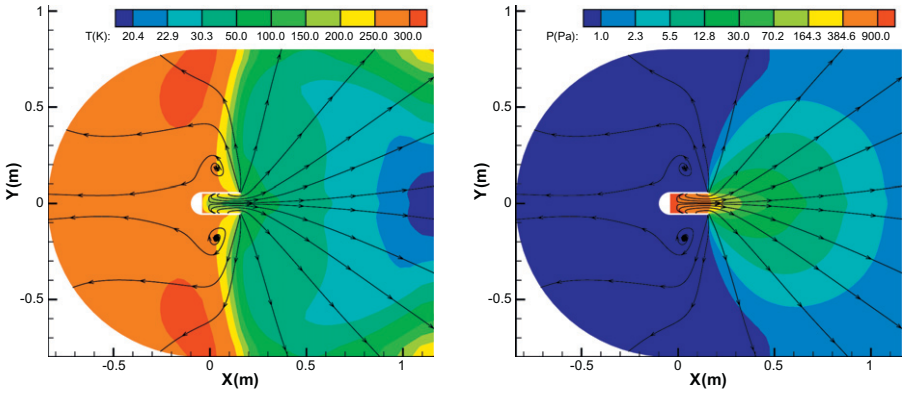

Fig. 16. The flow field during expansion stage.

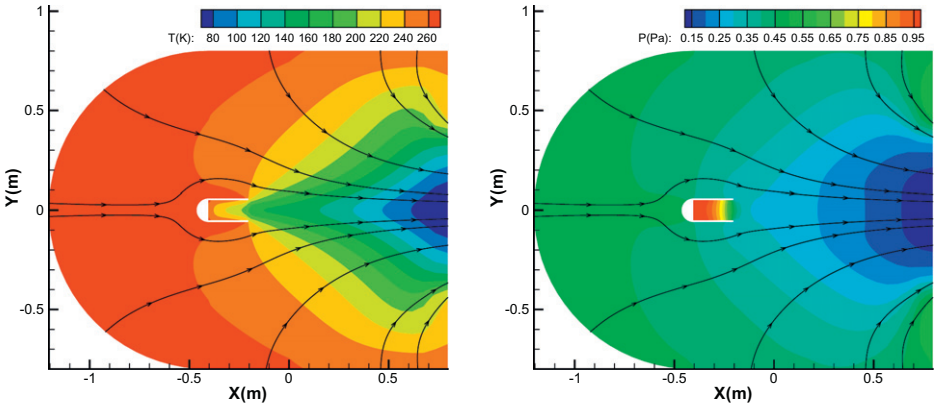

Fig. 17. The jet-like flow field.

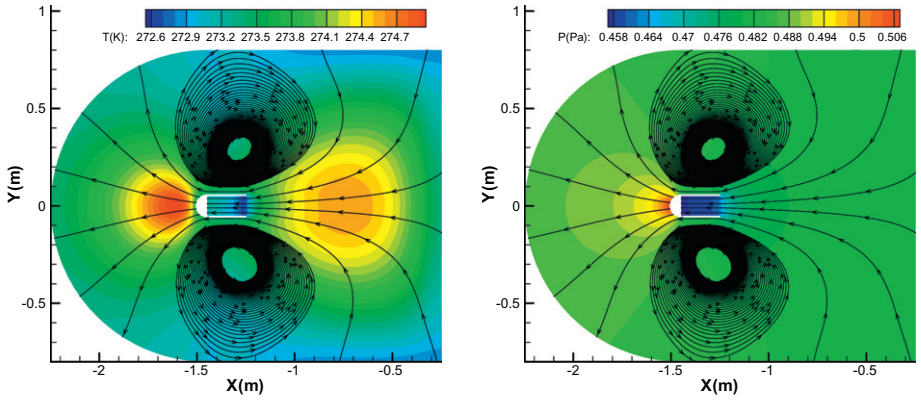

Fig. 18. The flow field during deceleration stage.

of nozzle is about 37.3 m/s moving toward to the left. The force in the x direction indicates that the acceleration process lasts a very short period. After accelerating process, the deceleration takes effect. The simulation of the decelerating flight process becomes simpler than the early stage. Theoretically, a conventional CFD method with slip boundary condition may be sufficient for the later stage.

For the AUGKS, the mesh is concentrated in the area where particles accumulate, as shown in this section. For the shock driven ellipse, the AUGKS is about four times faster than the UGKS when a uniform mesh in the velocity space is used. The UGKS requires 64×64 velocity elements to achieve the same accuracy, where the AUGKS only uses 760 velocity elements.

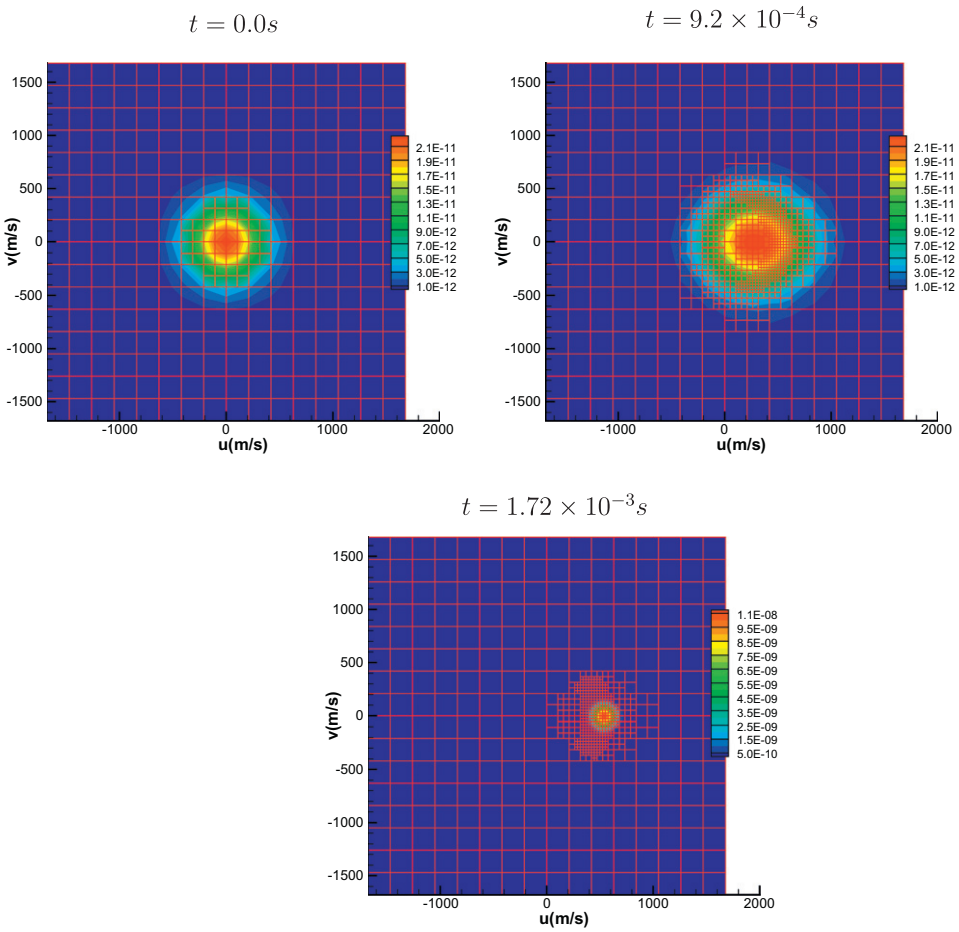

Fig. 19. The typical distribution function at the middle of the right outlet.

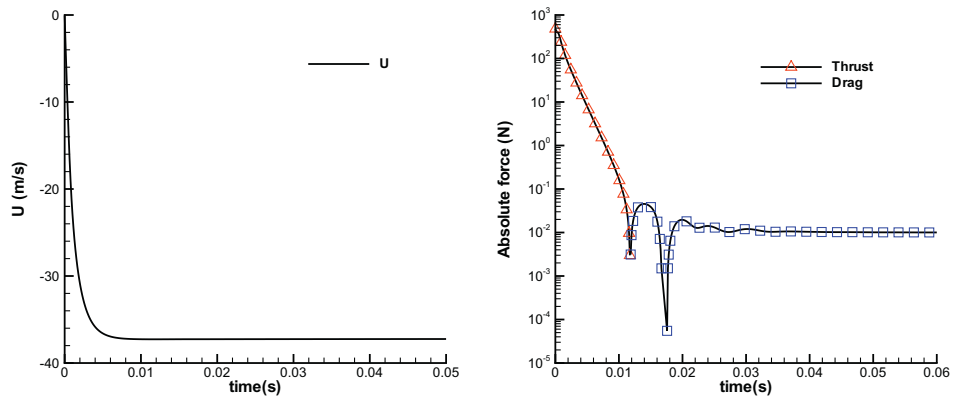

Fig. 20. The time series of the velocity and absolute force in x direction of nozzle.

The additional storage and load for quadtree structure are less than 20%. For the nozzle case, the extreme low temperature limits the finest mesh size in the velocity space. According to velocity mesh in Fig. 19, for the same accuracy a uniform mesh with 256×256 grid points is necessary. This number is much larger than 1300 velocity elements used in the AUGKS calculation. In this paper, the route of mesh refinement may not be an optimized one. As shown in this section, the mesh does not follow the density of particles precisely, and the mesh depends on the refining history. This kind of optimization problem can be partially solved by a global monitor function for the mesh adaptation, which is a research topic for the future.

5. Conclusion

The UGKS is a PDE-based modeling scheme. The success is mainly due to the use of the integral solution (9), which covers both hydrodynamic and kinetic scale flow physics. Meanwhile, the conservation law is implemented in the updates of both macroscopic and microscopic flow variables. Since the UGKS is not targeting to solve any specific kinetic equation, the role of the equation is used to construct a physical processes for the flow evolution around a cell interface. The physics recovered locally through the modeling is of significance to represent a physical reality in different scales. For a sophisticated particle collision, the gain term g^+ can be further modified. Different from other kinetic solvers, through this local integral solution, the UGKS couples the particle collision and transport. This coupling not only enlarges the time step, but also simplifies the collision term. Following this philosophy, the boundary condition which depends on the Knudsen number is also proposed. Moreover, the UGKS, similar to other Boltzmann-type solvers, is free of statistical fluctuation.

The adaptive UGKS is proposed in this paper through the introduction of moving mesh and adaptive quadtree velocity space into the scheme. Moving mesh technique enables the UGKS to simulate a moving solid–gas interaction. The adaptive quadtree velocity space improves the efficiency of the UGKS. Several constraints have been proposed to reduce the numerical error due to particle switching among different velocity levels. Two challenge test cases have been presented, which demonstrate the capabilities of AUGKS for high speed rarefied flow computations.

As claimed by Bird [3], the bottle-neck for a direct Boltzmann solver in aerospace application is the discretization of a large particle velocity space and the calculation of the complicated particle collision term. The use of adaptive mesh in the velocity space partially releases the burden imposed on the Boltzmann solver. The use of kinetic model eliminates the excessive computational cost for the evaluation of the exact Boltzmann collision term. Even with the simplified collision model, the numerical tests presented in this paper and these in all previous publications clearly demonstrate that the UGKS is an accurate flow solver in all Knudsen number flow regimes. So far, we have not encountered a single case which could fail the UGKS. The advantage of the UGKS is even more obvious in the low speed micoflow computations due to its absence of statistical scattering and its smooth transition between rarefied and hydrodynamic flow regimes.

Acknowledgments

This work was supported by the National Natural Science Foundation of China under Grant No.109103010062 and the National Foundation for Distinguished Young Scholar of China under Grant No. 10525208. This work was also supported by the National Climb-B Plan under Grant No. 2009CB724100 and the National Natural Science Funds for Distinguished Young Scholar group under Grant No.10921202. Additional support is from Hong Kong Research Grant Council 621709, 621011, HKUST SRFI11SC05, RPC10SC11, and National Key Basic Research Program (2009CB724101).

References

[1] G.A. Bird, Approach to translational equilibrium in a rigid sphere gas, Phys. Fluids 6 (1963) 1518.
[2] G.A. Bird, Monte carlo simulation of gas flows, Annu. Rev. Fluid Mech. 10 (1) (1978) 11–31.
[3] G.A. Bird, Molecular Gas Dynamics and the Direct Simulation of Gas Flows, Clarendon Press, Oxford, 1994.
[4] H. Grad, On the kinetic theory of rarefied gases, Commun. Pure Appl. Math. 2 (1949) 331–407.
[5] H. Struchtrup, M. Torrilhon, Regularization of grad's 13 moment equations: derivation and linear analysis, Phys. Fluids 15 (2003) 2668.
[6] X. Gu, D.R. Emerson, A high-order moment approach for capturing non-equilibrium phenomena in the transition regime, J. Fluid Mech. 636 (2009) 177–216.
[7] D. Burnett, The distribution of velocities in a slightly non-uniform gas, Proc. Lond. Math. Soc. 39 (1935) 385–430.
[8] K. Xu, Regularization of the chapman-enskog expansion and its description of shock structure, Phys. Fluids 14 (2002) L17–L20.
[9] M. Torrilhon, H. Struchtrup, Regularized 13-moment equations: shock structure calculations and comparison to Burnett models, J. Fluid Mech. 513 (2004) 171–198.
[10] T. Ohwada, K. Xu, The kinetic scheme for full Burnett equations, J. Comput. Phys. 201 (2004) 315.
[11] K. Xu, Z. Li, Microchannel flows in slip flow regime: BGK-Burnett solutions, J. Fluid Mech. 513 (2004) 87.
[12] K. Xu, Super-Burnett solutions for poiseuille flow, Phys. Fluids 15 (7) (2003) 2077.
[13] X. Zhong, R.W. MacCormack, D.R. Chapman, Stabilization of the Burnett equations and application to hypersonic flows, AIAA J. 31 (1993) 1036–1043.
[14] T.E. Schwartzentruber, I.D. Boyd, A hybrid particle-continuum method applied to shock waves, J. Comput. Phys. 215 (2006) 402–416.
[15] T.E. Schwartzentruber, L.C. Scalabrin, I.D. Boyd, Hybrid particle-continuum simulations of hypersonic flow over a hollow-cylinder-flare geometry, AIAA J. 46 (2008) 2086.
[16] J.M. Burt, I.D. Boyd, A hybrid particle approach for continuum and rarefied flow simulation, J. Comput. Phys. 228 (2009) 460–475.
[17] F. La Torre, S. Kenjeres, C.R. Kleijn, J.-L.P.A. Moerel, Evaluation of micronozzle performance through DSMC, Navier-Stokes and coupled DSMC/Navier-Stokes approaches, in: Computational Science-ICCS, Lecture Notes in Computer Science, vol. 5544, Springer, Berlin/ Heidelberg, 2009, pp. 675–684.
[18] A. Nordsieck, B.L. Hicks, Monte carlo evaluation of the Boltzmann collision integral, Rarefied Gas Dynam. 5 (1967) 695–710.
[19] S.M. Yen, Monte carlo solutions of nonlinear Boltzmann equation for problems of heat transfer in rarefied gases, Int.J. Heat Mass Trans. 14 (1971) 1865–1869.
[20] F.G. Tcheremissine, Solution to the Boltzmann kinetic equation for high-speed flows, Comput. Math. Math. Phys. 46 (2) (2006) 315–329.
[21] N. Crouseilles, P. Degond, M. Lemou, A hybrid kinetic/fluid model for solving the gas dynamics Boltzmann-BGK equation, J. Comput. Phys. 199 (2) (2004) 776–808.
[22] V. Kolobov, R. Arslanbekov, V. Aristov, A. Frolova, S. Zabelok, Unified solver for rarefied and continuum flows with adaptive mesh and algorithm refinement, J. Comput. Phys. 223 (2007) 589–608.
[23] J.Y. Yang, J.C. Huang, Rarefied flow computations using nonlinear model Boltzmann equations, J. Comput. Phys. 120 (1995) 323–339.
[24] Z.-H. Li, H.-X. Zhang, Study on gas kinetic unified algorithm for flows from rarefied transition to continuum, J. Comput. Phys. 193 (2004) 708–738.
[25] Z.-H. Li, H.-X. Zhang, Gas-kinetic numerical studies of three-dimensional complex flows on spacecraft re-entry, J. Comput. Phys. 228 (2009) 1116–1138.
[26] K. Xu, J.-C. Huang, A unified gas-kinetic scheme for continuum and rarefied flows, J. Comput. Phys. 229 (2010) 7747–7764.

[27] K. Xu, J.-C. Huang, An improved unified gas-kinetic scheme and the study of shock structures, IMA J. Appl. Math. 76 (2011) 698–711.
[28] J. Huang, K. Xu, P. Yu, A unified gas-kinetic scheme for continuum and rarefied flows ii: Multi-dimensional cases, Commun. Comput. Phys. 3 (3) (2012) 662–690.
[29] J. Huang, K. Xu, P. Yu, A unified gas-kinetic scheme for continuum and rarefied flows iii: Microflow simulations, preprint.
[30] M. Gutnic, M. Haefele, I. Paun, E. Sonnendrcker, Vlasov simulations on an adaptive phase-space grid, Comput. Phys. Commun. 164 (2004) 214–219.
[31] M. Mehrenberger, E. Violard, O. Hoenen, M.C. Pinto, E. Sonnendrücker, A parallel adaptive Vlasov solver based on hierarchical finite element interpolation, Nuclear Instrum. Methods Phys. Res. A 558 (2006) 188–191.
[32] V.I. Kolobov, R.R. Arslanbekov, A.A. Frolova, Boltzmann solver with adaptive mesh in velocity space, 27th International Symposium on Rarefied Gas, Dynamics 133 (2010) 928–933.
[33] V.I. Kolobov, R.R. Arslanbekov, Towards adaptive kinetic-fluid simulations of weakly ionized plasmas, J. Comput. Phys. 231 (3) (2012) 839–869.
[34] C.K. Chu, Kinetic-theoretic description of the formation of a shock wave, Phys. Fluids 8 (1) (1965) 12–22.
[35] K. Xu, A gas-kinetic BGK scheme for the Navier-Stokes equations and its connection with artificial dissipation and Godunov method, J. Comput. Phys. 171 (2001) 289–335.
[36] C. Jin, K. Xu, A unified moving grid gas-kinetic method in eulerian space for viscous flow computation, J. Comput. Phys. 222 (2007) 155–175.
[37] G.A. Bird, Aspects of the structure of strong shock waves, Phys. Fluids 13 (1970) 1172–1177.
[38] G.J. Maslach, S.A. Schaaf, Cylinder drag in the transition from continuum to free molecule flow, Phys. Fluids 6 (1963) 315.
[39] H.M. Mott-Smith, The solution of the Boltzmann equation for a shock wave, Phys. Rev. 82 (1951) 885.